Journal of the European Ceramic Society **9** (1992) 19–25

Densification of $0{\cdot}99SnO_2$–$0{\cdot}01CuO$ Mixture: Evidence for Liquid Phase Sintering

Nathalie Dolet, Jean-Marc Heintz, Marc Onillon & Jean-Pierre Bonnet

Laboratoire de Chimie du Solide du CNRS, 351, Cours de la Libération, 33405 Talence Cédex, France

(Received 11 January 1991; revised version received 22 May 1991; accepted 13 June 1991)

Abstract

The sintering of a $0{\cdot}99SnO_2$–$0{\cdot}01CuO$ molar mixture was studied at 1150°C in air. A fast and high densification was observed: the compactness obtained can reach 98·7%. After grain rearrangement, the simultaneous changes in shrinkage and grain size observed versus time were in agreement with a liquid phase sintering mechanism.

It was shown that copper dissolves into the SnO_2 rutile type structure. The electrical behaviour of the material obtained was in agreement with an interstitial position for copper ions.

Das Sinterverhalten einer $0{\cdot}99SnO_2$–$0{\cdot}01CuO$ Mischung wurde bei 1150°C in Luft untersucht. Dabei wurde eine hohe Sintergeschwindigkeit mit einer hohen Enddichte beobachtet: es können Enddichten bis zu 98·7% erreicht werden. Nach einer anfänglichen Umlagerung der Körner konnte mittels paralleler Verfolgung der Schwindung und der Korngröße als Funktion der Versuchszeit auf einen Flüssigphasensintermechanismus geschlossen werden. Es konnte nachgewiesen werden, daß sich das Kupfer in der Rutil-Struktur des SnO_2 löst. Auch die elektrischen Eigenschaften des gewonnenen Werkstoffs lassen auf eine interstitielle Position des Kupferions schließen.

Le frittage à l'air à 1150° d'un mélange de composition molaire $0{\cdot}99SnO_2$–$0{\cdot}01CuO$ conduit à une densification rapide résultant de l'apparition d'un liquide riche en cuivre à $T > 1092°C$.

Au début du frittage un réarrangement des grains se produit. Les phénomènes observés ensuite sont paramètrés en utilisant le modèle de frittage en phase liquide. Par ailleurs, pendant le traitement thermique le cuivre se dissout dans le réseau rutile de SnO_2. Le comportement électrique suggère l'insertion du cuivre en site interstitiel.

1 Introduction

The densification of pure SnO_2 can be strongly limited by the vaporization of tin monoxide[1] which should occur at a high rate above 1100°C according to the reaction:

$$SnO_2(s) \rightarrow SnO(g) + \tfrac{1}{2}O_2(g) \qquad (1)$$

Nevertheless dense tin dioxide based ceramics can be obtained using natural sintering with the help of additives such as MnO_2, CuO, ZnO, Li_2CO_3.[2–4] The role of these additives has not yet been clearly established. For example in the case of CuO, the most efficient of them, two different mechanisms have been proposed. On the one hand Duvigneaud & Reihnard[4] have suggested the formation of a liquid phase. On the other hand Varela *et al.*[2] have considered the effect of an increase in the oxygen diffusion rate in SnO_2 due to the formation of oxygen vacancies according to (2) (using the Kröger and Vink formalism[5]):

$$CuO \xrightarrow{SnO_2} Cu_{Sn}^{2'} + O_o^x + V_o^{2\cdot} \qquad (2)$$

Our purpose in this paper is to determine the nature of the high temperature sintering mechanism(s) of tin dioxide in the presence of CuO and to localize copper in the ceramics.

2 Material Elaboration

This paper deals only with results concerning the $0{\cdot}99SnO_2$–$0{\cdot}01CuO$ molar composition which leads after sintering to a maximum in ceramic density (Fig. 1). The basic materials used were SnO_2 (Aldrich 99·9%) with a specific surface area of

Journal of the European Ceramic Society 0955–2219/92/$5.00

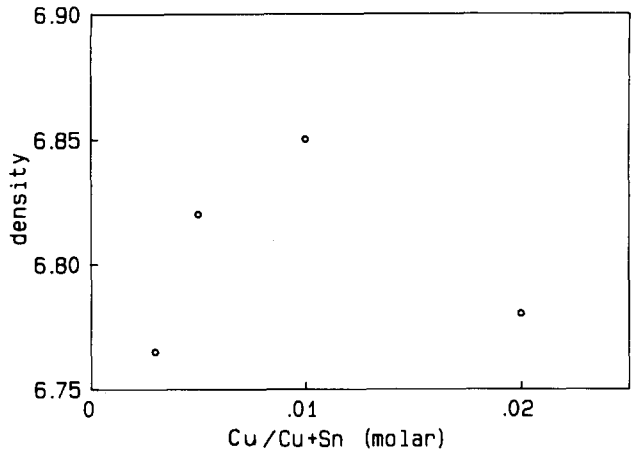

Fig. 1. Influence of the initial amount of CuO on the final density of SnO_2-based ceramics sintered in air at 1150°C for 1 h.

7·33 $m^2\ g^{-1}$ and CuO (Prolabo Normapur 99%) with a specific surface area of 14·8 $m^2\ g^{-1}$.

The two appropriate quantities of powders were mixed in an agate mortar in the presence of pure ethanol. After drying and calcining for 3 h in air at 400°C the powders were pressed under a uniaxial pressure of 100 MPa to obtain cylindrical samples (6 mm or 8 mm diameter and about 2·5 mm thickness). The green density of these samples was about 2·8 $g\,cm^{-3}$. Some of the samples were then sintered in air at 1150°C for a holding time in the 0·25–15 h range. After sintering the ceramics were always cooled in 10 min.

3 Material Characterization

3.1 Densification characterization

The shrinkage rates have been followed using a NETZSCH differential dilatometer. Two types of study were performed in air on the cylinders prepared as described previously:

(i) The sample was heated at 200°C h^{-1} up to 1150°C and held for 15 h at this temperature.
(ii) The samples were quickly heated (in 5 min) to 1150°C and held for 80 min at this temperature in order to follow the beginning of the isothermal shrinkage.

The apparent density of the ceramics obtained was determined using the Archimedes method according to the British Standard 1902.[6]

3.2 Microstructure characterization

The average grain size in the various ceramics was estimated from SEM micrographs of samples polished and then thermally etched (1100°C, 15 min).[7]

In order to vizualize possible intergranular phases thin slices of ceramics were observed using a JEOL 1200 CX scanning transmission electron microscope (STEM) with an accelerating voltage of 120 kV. The slices were prepared by polishing down to 40 μm followed by ion beam thinning using argon (accelerating voltage: 5 kV).

Chemical analyses were performed on polished or fractured samples using electron or Auger microprobes.

3.3 Electrical properties

The electrical conductivity of some ceramics was determined in air between 20 and 1000°C using a four probe method with platinum leads and contacts. The values quoted are those observed during cooling.

4 Results and Discussion

4.1 Sintering behaviour of 0·99SnO_2–0·01CuO mixture

For a given sintering time, t_s, the density of the ceramics obtained from a molar 0·99SnO_2–0·01CuO mixture is strongly sensitive to the sintering temperature T_s (Fig. 2); highly densified ceramics can be obtained when $T_s \geq 1000$°C. The maximum densification is observed for $T_s = 1150$°C and the study presented here deals mainly with this sintering temperature.

4.2 Kinetics of isothermal sintering at 1150°C

Figure 3 presents the evolution of the logarithm of the relative shrinkage ($\Delta L/L_0$) as a function of $\ln(t_s)$ observed during isothermal dilatometry performed at 1150°C. The densification process appears to be very fast: 94% density is obtained after a holding time, t_s, as short as 8 min. The evolution of the $\ln(\Delta L/L_0) = f(\ln(t_s))$ curve presents two linear parts

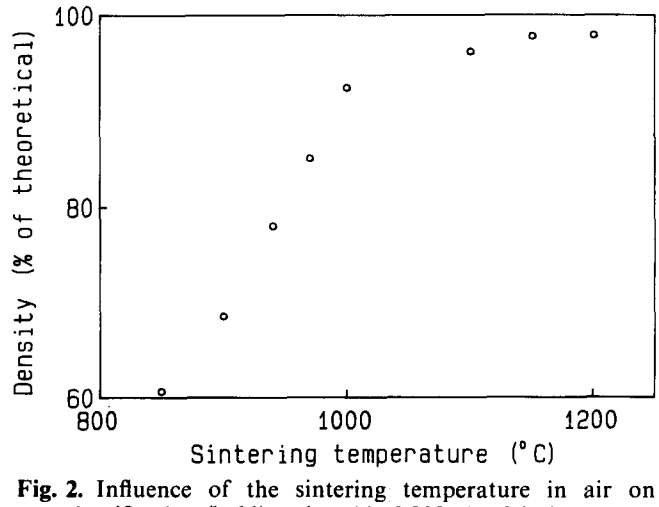

Fig. 2. Influence of the sintering temperature in air on densification (holding time 1 h, 0·99SnO_2–0·01CuO).

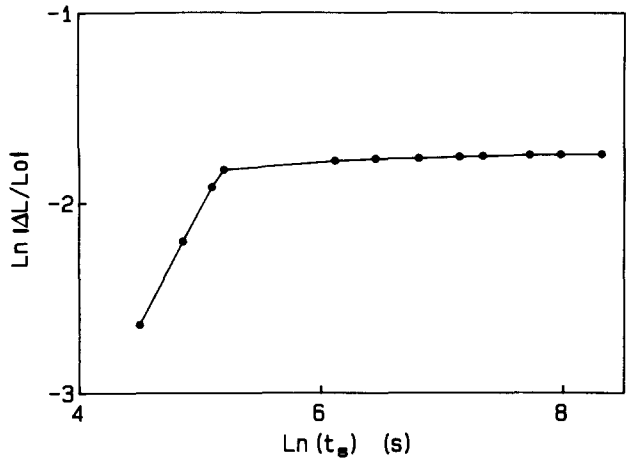

Fig. 3. Evolution of the relative shrinkage versus time for SnO_2-based ceramics heated in air at 1150°C (0·99SnO_2–0·01CuO).

with respective slopes $p_1 = 1{\cdot}20 \pm 0{\cdot}05$ for $0 < t < 7$ min and $p_2 = 0{\cdot}05 \pm 0{\cdot}02$ for $7 < t < 80$ min.

The fast shrinkage observed during the first sintering step ($t_s < 7$ min, p_1 $1{\cdot}20 \pm 0{\cdot}02$) cannot be described by one of the usual sintering models. This behaviour can be the result of grain rearrangement[8] possibly accelerated by the presence of a liquid phase acting as a lubricant. The existence of such a phase at high temperature is revealed by the presence of copper-rich coagulated droplets on the surface of the sample sintered for 1 h at 1150°C, then heated for 30 min at 1100°C (Fig. 4).

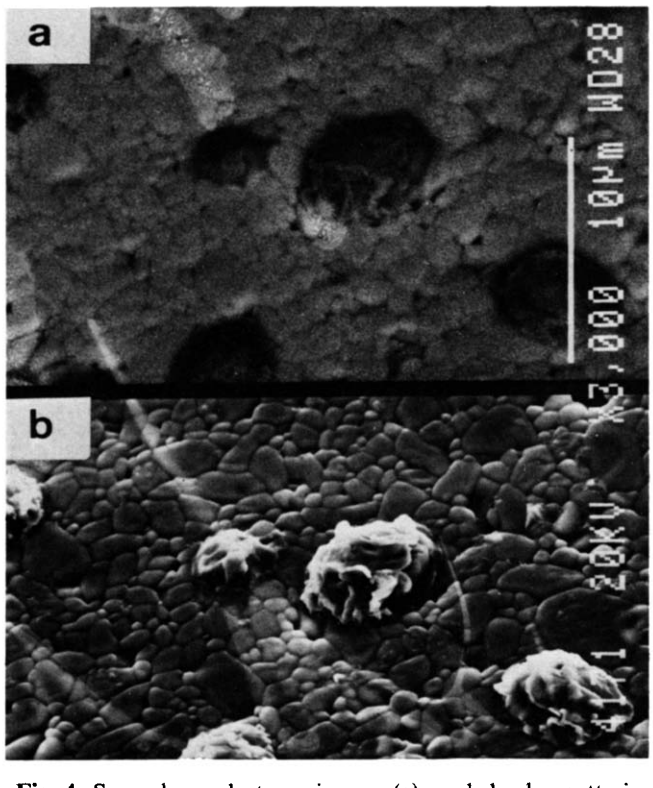

Fig. 4. Secondary electron image (a) and back scattering electron image (b) of the surface of ceramics sintered in air for 1 h at 1150°C, then heated for 30 min at 1100°C (0·99SnO_2–0·01CuO).

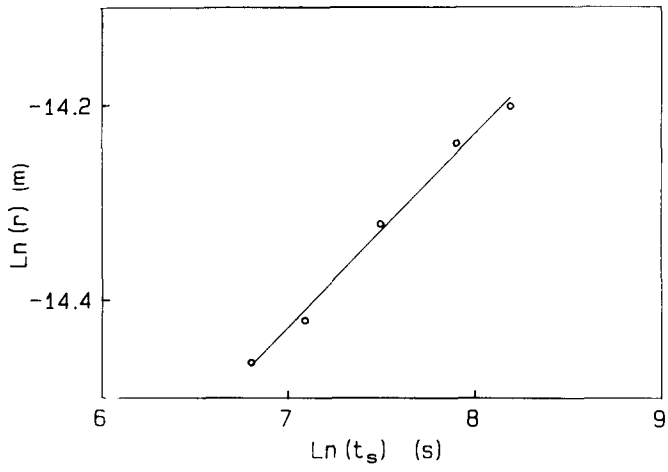

Fig. 5. Evolution with time of the average grain radius r in ceramics heated in air at 1150°C (0·99SnO_2–0·01CuO).

If the liquid phase is still present once the grain rearrangement step is completed, densification can then be controlled by a liquid phase sintering mechanism.

According to Ref. 8, if the diffusion is the limiting process in mass transfer, the shrinkage evolution can be described by the relation:

$$\Delta L/L_0 = A(r)^{-4/3}(t)^{1/3} \tag{3}$$

where A is a constant and r the average grain radius.

If dissolution at the solid–liquid interface[8] is the limiting process, the following expression must then be considered:

$$\Delta L/L_0 = B(r)^{-1}(t)^{1/2} \tag{4}$$

where B is a constant.

The evolution of the average grain radius with sintering time, t_s, is reported in Fig. 5. A linear variation of $\ln(r)$ versus $\ln(t_s)$ is observed. As the corresponding slope is $p = 0{\cdot}20 \pm 0{\cdot}02$ the following relation can be written:

$$r = C(t)^{1/5} \tag{5}$$

where C is a constant. Such a variation is the same as that generally used to describe grain growth controlled by either grain boundary impurities or intergranular phase.[9] Combining these experimental variations of r with relations (3) and (4), the following expressions are obtained:

(i) liquid phase sintering controlled by diffusion

$$\Delta L/L_0 = D(t)^{1/15} \tag{6}$$

(ii) liquid phase sintering controlled by dissolution

$$\Delta L/L_0 = E(t)^{3/10} \tag{7}$$

where D and E are constants.

As the p_2 value ($0{\cdot}05 \pm 0{\cdot}02$) is very close to 0·067 (1/15), the experimental evolution of $\ln(\Delta L/L_0)$

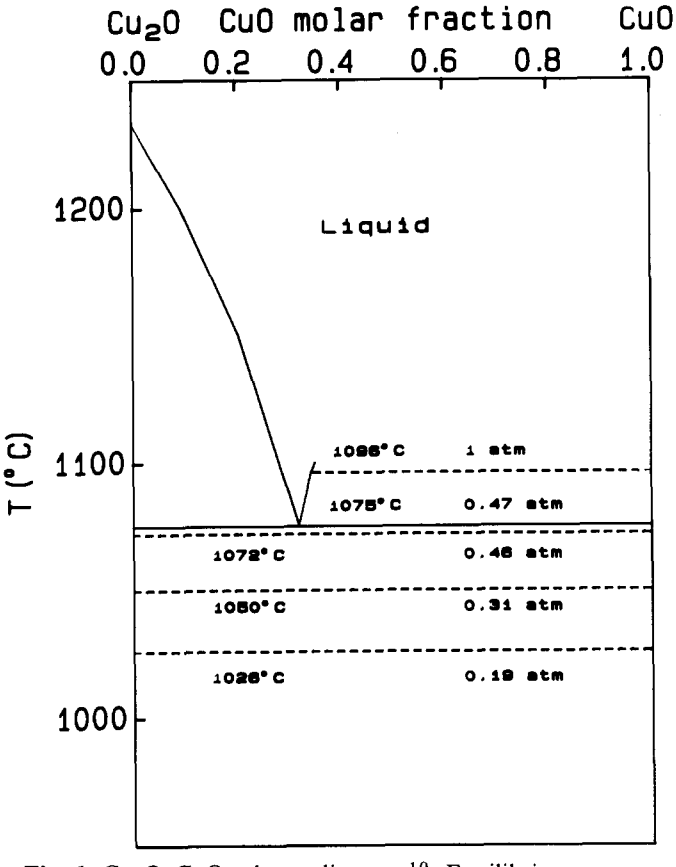

Fig. 6. Cu_2O–CuO phase diagram.[10] Equilibrium oxygen partial pressures are reported for several temperatures.

versus $\ln(t_s)$ observed for $t_s > 7$ mn can be described by relation (6).

The experimental results indicate that the densification of SnO_2 with a small amount of CuO at 1150°C is mainly due to the presence of a liquid phase. This phase favours the particle rearrangement in a first step (first part of the $\Delta L/L_0$ curve in Fig. 3), and then controls the sintering through a mechanism in which the limiting phenomenon is the diffusion in the liquid.

4.3 Thermodynamic conditions for the existence of a liquid in the Cu(s)–O_2(g) system

The Cu_2O–CuO phase diagram (Fig. 6) obtained combining the data of Ref. 10 and thermodynamic calculations shows that eutectic equilibrium exists at $T_E = 1075°C$ for $pO_2 = 0{\cdot}47$ atm. The evolution of the nature of the phases present at higher temperatures ($T > T_E$) under different pO_2 can be understood with the help of an isothermal Gibbs energy–composition diagram for the Cu(s)–O_2(g) system (Fig. 7).

At this temperature, the common tangent to the CuO and liquid phase curves defines the liquid composition Cu_xO and the oxygen partial pressure $p^{\alpha}O_2$ corresponding to the following equilibrium:

$$2/(\alpha-1)Cu_xO_{(liq)} + O_{2(g)} \rightleftharpoons 2\alpha/(\alpha-1)CuO_{(s)} \quad (8)$$

In the same way, the common tangent to the Cu_2O(s) and liquid phase curves defines the liquid composition $Cu_\beta O$ and $p^{\beta}O_2$ corresponding to the following equilibrium:

$$2\beta/(2-\beta)Cu_2O_{(s)} + O_{2(g)} \rightleftharpoons 4/(2-\beta)Cu_\beta O_{(liq)} \quad (9)$$

For $p^{\alpha}O_2 > pO_2 > p^{\beta}O_2$ the stable condensed phase is liquid. Unfortunately all the data related to this liquid phase which are required for the determination of $p^{\alpha}O_2$ and $p^{\beta}O_2$ are not available. Nevertheless the standard Gibbs energies of formation of $CuO_{(s)}$ and $Cu_2O_{(s)}$ are known at all temperatures[11]

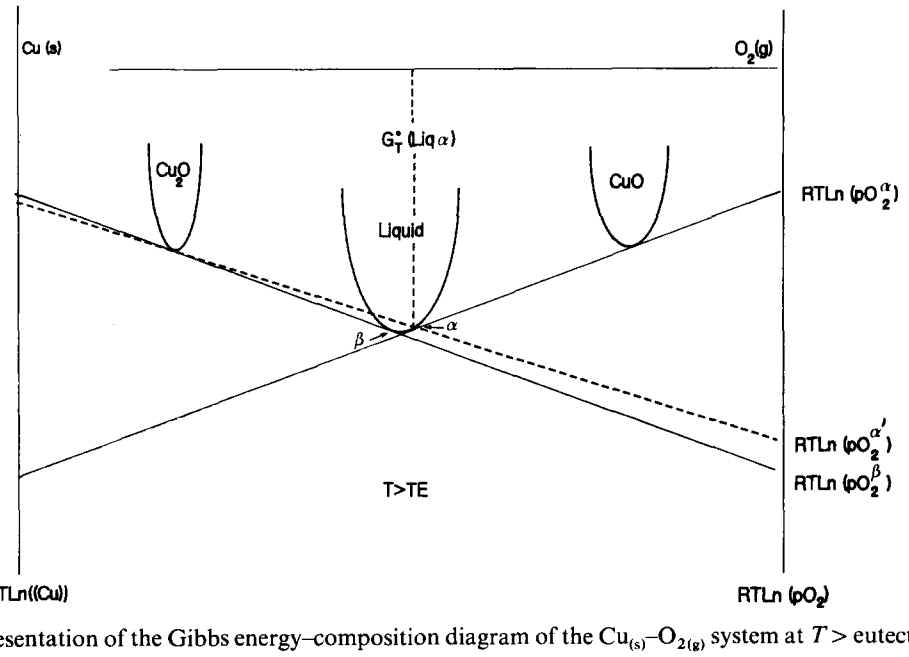

Fig. 7. Qualitative representation of the Gibbs energy–composition diagram of the $Cu_{(s)}$–$O_{2(g)}$ system at $T >$ eutectic temperature T_E.

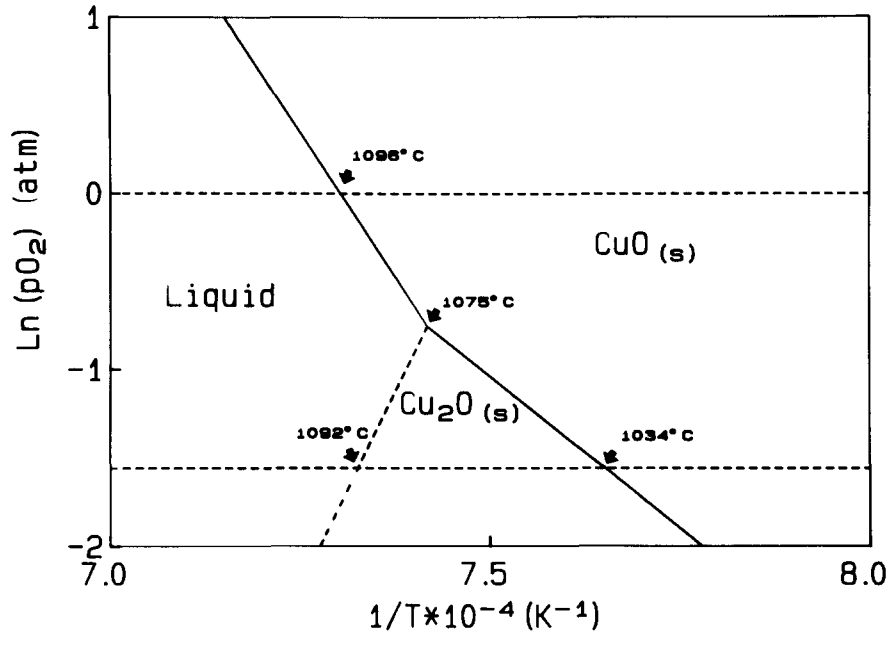

Fig. 8. Influence of temperature and oxygen partial pressure on phase stability in the copper–oxygen system.

and the liquid compositions $Cu_\alpha O$ and $Cu_\beta O$ can be determined between 1075 and 1100°C from the phase diagram (Fig. 6).

Under eutectic equilibrium conditions, solid CuO and Cu_2O can coexist and the partial pressure corresponding to the equilibrium:

$$2Cu_2O_{(s)} + O_{2(g)} \rightleftharpoons 4CuO_{(s)} \qquad (10)$$

can be calculated using thermodynamic data. At $T_E = 1075°C$, this pO_2 (0·47 atm) is equal to $p^\alpha O_2$ and $p^\beta O_2$.

At 1096°C the phase diagram (Fig. 6) indicates $p^\alpha O_2 = 1$ atm and the liquid α corresponds to a Cu/O molar fraction = 1·658. The value of $\Delta_f G^\circ_{1096\,°C}(\text{liq}\alpha)$ can be determined:

$$\begin{aligned}\Delta G^\circ_{1096\,°C}(8) &= RT\ln 1 \\ &= 5{\cdot}039\Delta_f G^\circ_{1096\,°C}(CuO_{(s)}) \\ &\quad - 3{\cdot}039\Delta_f G^\circ_{1096\,°C}(\text{liq}\alpha)\end{aligned}$$

Using this value (16·110 kJ mol^{-1}) and $\Delta_f G^\circ_{1096\,C}(Cu_2O_{(s)})$ it is possible to determine partial pressure $p^{\alpha'}O_2 = 0{\cdot}16$ atm corresponding to a hypothetical equilibrium between $Cu_2O_{(s)}$ and the liquid α at 1096°C. The true equilibrium (9) which involves at 1096°C a liquid β (with a Cu/O molar fraction = 1·71) corresponds to unknown $p^\beta O_2$. As illustrated by Fig. 7, $p^{\alpha'}O_2$ must be slightly higher than $p^\beta O_2$, then for $p^{\alpha'}O_2 \leq pO_2 \leq p^\alpha O_2$ a liquid phase must exist.

Considering that both the reaction entropy and the enthalpy variations are practically temperature independent, the variation of $\ln(p^\alpha O_2)$ and $\ln(p^{\alpha'}O_2)$ are linear versus reciprocal temperature (Fig. 8). The lower temperature at which a liquid phase occurs is strongly dependent on pO_2. In air a liquid exists at a temperature higher than 1092°C.

Though the presence of tin dioxide could modify this temperature it seems reasonable to consider the sintering of a 0·99SnO_2–0·01CuO mixture at 1150°C to be the result of the formation of a copper-rich liquid.

4.4 Evolution of the microstructure

For short times copper appears mainly located in an intergranular phase around the grains (Fig. 9). The nature of the first solid copper oxide to appear when cooling the liquid, after sintering, depends on the oxygen partial pressure as shown in Fig. 8. In air, Cu_2O which appears at first can be oxidized to CuO at lower temperatures than 1034°C. Such a transformation which is associated with a 5% volume

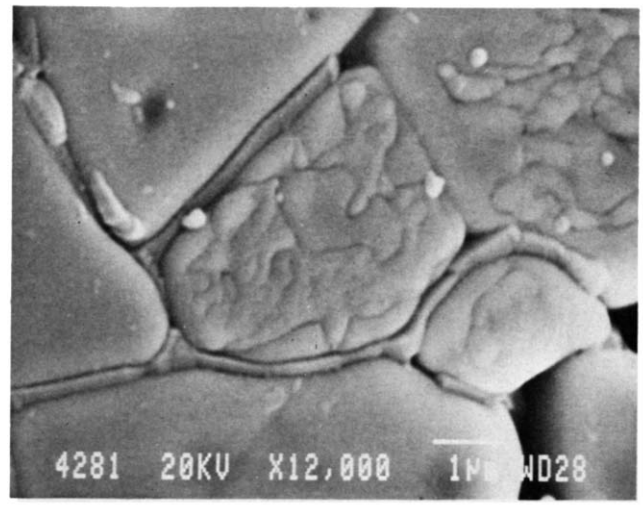

Fig. 9. Intergranular phase in ceramics sintered in air for 30 min at 1150°C and quenched.

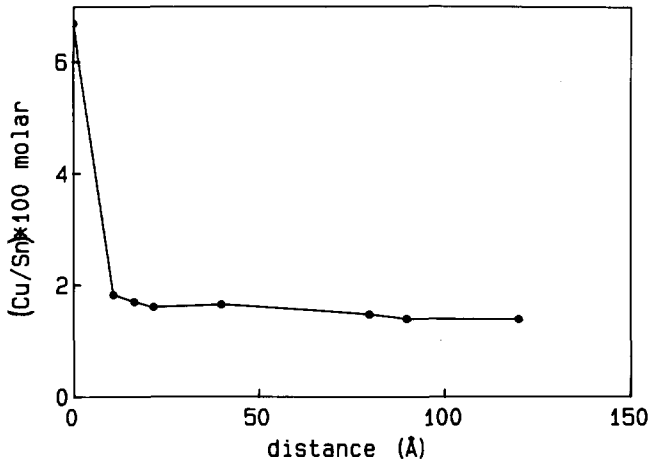

Fig. 10. Copper concentration profile through a grain in ceramics ($0{\cdot}99SnO_2$–$0{\cdot}01CuO$) sintered for 8 h at 1150°C in air (origin at the grain surface).

increase can generate stresses and microdeformations within the microstructure. As this oxidation process is slow, it appears then that both the atmospheric composition and the cooling rate after sintering can strongly influence the intergranular layer composition and the texture of a tin oxide ceramic sintered in the presence of copper oxide at 1150°C.

The solubility of copper in the tin dioxide grains was studied using an Auger microprobe. Figure 10 illustrates the evolution of copper concentration as a function of the distance from the surface of a grain located in the inner part of a ceramic sintered for 8 h at 1150°C in air. The $Cu/Sn \approx 1{\cdot}5\%$ molar ratio determined is higher than its average value in the ceramic ($Cu/Sn = 1\%$) as confirmed by electron microprobe. Thus the solubility of copper inside the grain is sufficient to consume progressively the whole liquid phase. It can be concluded from various observations that the amount of liquid phase

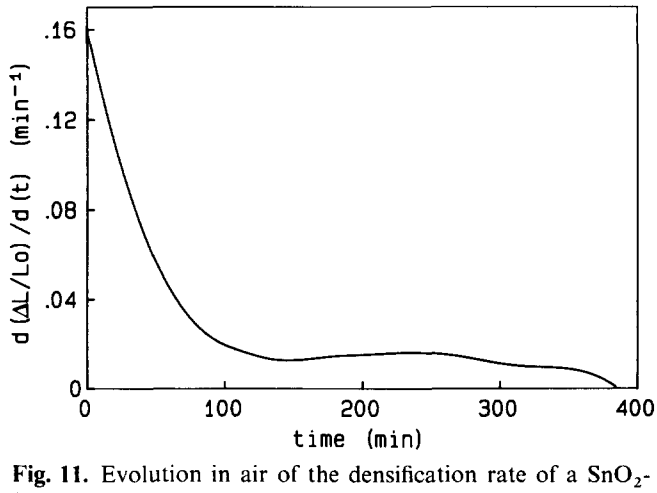

Fig. 11. Evolution in air of the densification rate of a SnO_2-based compact versus holding time at 1150°C ($0{\cdot}99SnO_2$–$0{\cdot}01CuO$).

remaining after more than 4 h sintering at 1150°C is negligible. For example, TEM examinations show that the grain boundaries are then free from any intergranular phase.

The densification observed for sintering times longer than 4 h (Fig. 11) must then be due to the intervention of a mechanism other than liquid phase sintering such as for example solid state diffusion.

4.5 Position of copper in the tin dioxide crystallographic network

Depending on the nature of the crystallographic sites occupied, copper dissolution in the rutile type network of SnO_2 can be described by different hypothetical reactions.

4.5.1 Substitution of Sn^{4+} by Cu^{2+}

Using the Kröger and Vink formalism,[5] the introduction of Cu^{2+} ions in Sn^{4+} positions can be written as follows:

$$CuO \xrightarrow{SnO_2} Cu'_{Sn} + O^x_o + V^{2\cdot}_o \qquad (2)$$

Simultaneously the following equilibrium exists:

$$O^x_o \rightleftharpoons \tfrac{1}{2}O_{2(g)} + 2e' + V^{2\cdot}_o \qquad (11)$$

with the constant of equilibrium:

$$K_{11} = k_{11}[V^{2\cdot}_o][e']^2(pO_2)^{1/2} \qquad (12)$$

At a given pO_2 the substitution of Sn^{4+} ions by Cu^{2+} ions is associated with an increase in oxygen vacancy concentration (2) and then to a decrease in the free electron concentration (12).

If we assume that the carrier mobility is not or is only weakly affected, the dissolution of copper must be linked to a decrease in the n type conductivity, σ_n, of pure SnO_2.

4.5.2 Copper in interstitial position

The insertion of copper into the rutile network can also be described by the dissolution reaction:

$$CuO \xrightarrow{SnO_2} Cu^{2\cdot}_i + O^x_o + \tfrac{1}{2}V^{4'}_{Sn} \qquad (13)$$

Considering the constant of the Schottky disorder equilibrium:

$$K_{14} = k_{14}[V^{2\cdot}_o]^2[V^{4'}_{Sn}] \qquad (14)$$

it appears that the insertion of copper interstitially into a tin dioxide network must be associated with an increase in tin vacancy concentration and a decrease of oxygen vacancy concentration. These oxygen vacancies are also involved in the equilibrium (11), which is associated with the constant:

$$K_{11} = k_{11}[V^{2\cdot}_o][e']^2(pO_2)^{1/2} \qquad (12)$$

Then at a given partial pressure of oxygen it appears

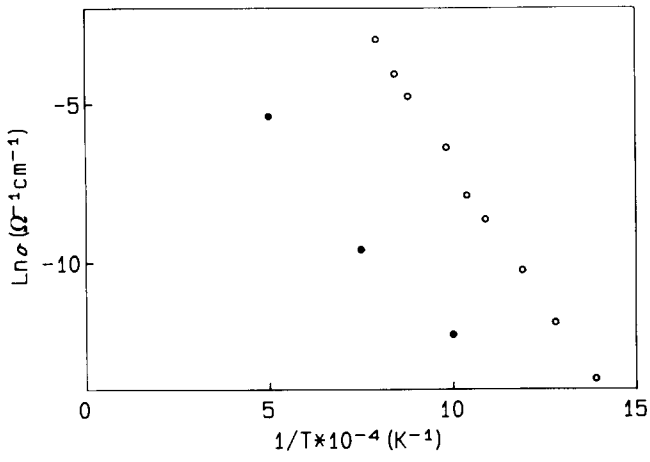

Fig. 12. Evolution of electrical conductivity versus reciprocal absolute temperature for: ●, SnO_2 crystal;[12] ○, SnO_2-based ceramics (0·99SnO_2–0·01CuO).

that interstitial copper in a tin dioxide network can result in an increase of free electron concentration and hence of the n type conductivity, σ_n, of pure SnO_2.

The thermoelectric power of our SnO_2-based ceramics measured in air between 600 and 900°C is negative. As this result indicates a n-type conductivity, the comparison between the conductivity in air of a pure SnO_2 single crystal and of 0·99SnO_2–0·01CuO ceramics should give information about the position of the copper in the tin dioxide network. The results reported in Fig. 12 indicate a higher conductivity for the ceramics and thus suggest an interstitial position for copper. In this discussion we have considered only the case of Cu^{2+} ions, the presence of Cu^+ or Cu^{3+} ions should not affect the nature of the evolution of the free electron concentrations in the two hypotheses described.

5 Conclusions

The sintering at 1150°C in air of a 0·99SnO_2–0·01CuO molar mixture leads to highly densified ceramics. As a liquid exists in air in the $Cu_{(s)}$–$O_{2(g)}$ system at temperatures higher than 1092°C, it can be assumed that the sintering is mainly due to a copper oxide-based liquid.

The first densification step is associated with grain rearrangement, the second one can be fitted by the usual relations available in the case of liquid phase sintering.

During sintering copper oxide can dissolve within the rutile type structure of SnO_2. The electrical behaviour of the material obtained was in agreement with an interstitial position for the copper ion.

Acknowledgements

The authors express thanks to Professor J. Etourneau for valuable discussions and L. Rabardel for dilatometric measurements.

References

1. Park, S. J., Hirota, K. & Yamamura, H., *Ceram. Int.*, **10** (1984) 116.
2. Varela, J. A., Whittemore, O. J. & Ball, M. J., *Sintering 85*, ed. G. C. Kuczynski *et al.* Elsevier, Washington, 1987, p. 256.
3. Grigoryan, L. T., Gedakyan, D. & Kostanyan, K. A., *Inorg. Mater.*, **12** (1976) 313.
4. Duvigneaud, P. H. & Reihnard, D., *Sci. Ceram.*, **12** (1980) 287–91.
5. Kröger, F. A. & Vink, H. J., *Solid State Physics*. Academic Press, New York, 1956, p. 307.
6. British Standard, BSS 1902, part 1A, BSI, London, 1966.
7. Case, E. O., Smyth, J. R. & Montei, V., *J. Am. Ceram. Soc.*, **64** (1981) C-24.
8. Kingery, W. D., *J. Appl. Phys.*, **30** (1969) 301.
9. Mocelin, A., *Surfaces and Interfaces of Ceramics Materials*, ed. L. C. Dufour, C. Monty and G. Petot-Evras. Kluwer Academic Publishers, Dordrecht, 1989, p. 485.
10. Levin, E. M., Robbison, C. R. & Mundie, H. Mc., *Phase Diagrams for Ceramists*, 1969 Supplements. American Ceramic Society Inc., New York, 1969.
11. Stull, D. R. & Prophet, H., *Janaf Thermochemical Tables*, 2nd edn. NSRDS-NBS37, 1971.
12. Jarzebski, Z. M. & Marton, J. P., *J. Electrochem. Soc.*, **9** (1976) 299.